Otology & Neurotology
39:e63–e73 © 2017, Otology & Neurotology, Inc.

An In-Vitro Insertion-Force Study of Magnetically Guided Lateral-Wall Cochlear-Implant Electrode Arrays

*Lisandro Leon, †Frank M. Warren, and ‡Jake J. Abbott

**Sarcos Robotics, Salt Lake City, Utah; †The Oregon Clinic, Portland, Oregon; and ‡Department of Mechanical Engineering, University of Utah, Salt Lake City, Utah*

Hypothesis: Insertion forces can be reduced by magnetically guiding the tip of lateral-wall cochlear-implant electrode arrays during insertion via both cochleostomy and the round window.

Background: Steerable electrode arrays have the potential to minimize intracochlear trauma by reducing the severity of contact between the electrode-array tip and the cochlear wall. However, steerable electrode arrays typically have increased stiffness associated with the steering mechanism. In addition, steerable electrode arrays are typically designed to curve in the direction of the basal turn, which is not ideal for round-window insertions, as the cochlear hook's curvature is in the opposite direction. Lateral-wall electrode arrays can be modified to include magnets at their tips, augmenting their superior flexibility with a steering mechanism. By applying magnetic torque to the tip, an electrode array can be navigated through the cochlear hook and the basal turn.

Methods: Automated insertions of candidate electrode arrays are conducted into a scala-tympani phantom with either a cochleostomy or round-window opening. The phantom is mounted on a multi-degree-of-freedom force sensor. An external magnet applies the necessary magnetic bending torque to the magnetic tip of a modified clinical electrode array, coordinated with the insertion, with the goal of directing the tip down the lumen. Steering of the electrode array is verified through a camera.

Results: Statistical *t*-test results indicate that magnetic guidance does reduce insertion forces by as much as 50% with certain electrode-array models. Direct tip contact with the medial wall through the cochlear hook and the lateral wall of the basal turn is completely eliminated. The magnetic field required to accomplish these insertions varied from 77 to 225 mT based on the volume of the magnet at the tip of the electrode array. Alteration of the tip to accommodate a tiny magnet is minimal and does not change the insertion characteristic of the electrode array unless the tip shape is altered.

Conclusion: Magnetic guidance can eliminate direct tip contact with the medial walls through the cochlear hook and the lateral walls of the basal turn. Insertion-force reduction will vary based on the electrode-array model, but is statistically significant for all models tested. Successful steering of lateral-wall electrode arrays is accomplished while maintaining its superior flexibility. **Key Words:** Cochlear hook—Insertion force reduction—Magnetic guidance—Robotic surgery—Steerable electrode.

Otol Neurotol **39:**e63–e73, 2018.

With increased focus on hearing preservation in cochlear implantation, especially given the benefits of combined electric-acoustic stimulation, methods to minimize intracochlear damage have become a priority in electrode placements. One approach has been to improve upon the insertion characteristics of the cochlear-implant electrode arrays (EAs). Design of lateral-wall (LW) EAs has considered parameters such as flexibility (1), dimensions (2), fabrication technique (3), and material selection (4). In general, LW EAs are designed to be thin and flexible so as to minimize trauma when the tip first contacts the LW of the cochlea.

Alternatively, perimodiolar EAs have a preformed curvature designed to curl away from the LW of the first turn. During insertion, the EA is advanced off its stylet so that the preformed shape functions as a steering mechanism. Proper technique requires the stylet to be stabilized at the appropriate distance from the cochleostomy (CO) site so that the electrode can avoid the LW while being advanced. If done correctly, negligible insertion forces can be achieved while eliminating tip contact with the LW (5–8). In practice, scalar excursion is a common occurrence with these perimodiolar EAs precisely at the location where it should be curling away

Address correspondence and reprint requests to Jake J. Abbott, Ph.D., Department of Mechanical Engineering, University of Utah, 1495 E 100 S, 1550 MEK, Salt Lake City, UT 84112; E-mail: jake.abbott@utah.edu

The content is solely the responsibility of the authors and does not necessarily represent the official views of the National Institutes of Health. The authors alone are responsible for the content and writing of the article.

Research reported in this publication was supported by the National Institute on Deafness and Other Communication Disorders of the National Institutes of Health under Award Number R01DC013168.

The authors disclose no conflicts of interest.

Supplemental digital content is available in the text.

DOI: 10.1097/MAO.0000000000001647

from the LW (9). This can happen if the stylet is stabilized deeper into the insertion than intended (10). It can also happen if torsion misaligns the electrode so that its tip curls into the basilar membrane (BM) (11).

In addition, hearing preservation has renewed interest in using the round window (RW) for electrode insertions (12–15) with the recent literature favoring the RW over a CO when hearing preservation is the primary consideration (16,17). Before the development of more flexible EAs, COs were favored because the stiffer multichannel EAs required a straight route into the lumen to avoid the cochlear hook (CH) region (18). In fact, the CH is problematic enough that several studies have examined the appropriate initial insertion vector needed for atraumatic results (15,19–22). The need to evaluate this initial vector is due to the proximity of the BM and osseous spiral lamina (OSL) to the RW opening, along with the challenge of guiding the EA tip satisfactorily down the lumen without first impacting these particular structures. For many, COs are still preferred because the insertion vector can be aligned with the lumen of the scala tympani (ST), making for easier insertions (17,23). However, this is becoming less of a concern with the recent trend toward more flexible and thinner LW EAs to reduce the effects of impact with intracochlear structures.

Although there are still many proponents of using COs (23), even when hearing preservation is desired (17), LW EAs are now routinely inserted through the RW, the primary benefit of which is direct entry into the ST, at the outset, with minimal drilling-related trauma (24). This is guaranteed because the ST terminates at the RW. In contrast, accurate placement of COs is mandatory to ensure initial ST insertions. Unfortunately, it has been shown that there is a 20% probability that the CO will be sited incorrectly by practicing surgeons, leading to potential EA misplacement into the scala vestibuli from the very outset (25). Even in cases where soft-surgery techniques are used, CO sites may be different than originally intended (26). Also, evidence from clinical practice indicates that using the RW for insertions produces a high percentage of complete ST placement (27), and EAs that are placed entirely within the ST tend to produce better hearing outcomes (28).

Recent evidence suggests that, unlike LW EAs, which are designed to be thin and flexible, perimodiolar EAs may not be very safe for RW insertions (11,29,30). A problem is that the stylet, which is needed to insert these devices, increases the overall thickness while reducing the flexibility, both of which are not suited for RW approaches and may make it more difficult for the electrode to pass through the CH (26,30).

Inspired by the steering capability of perimodiolar EAs, we have developed a method to navigate a LW EA by bending its tip away from the LW of the cochlea during insertion and, in the process, reduce the pressure along the entire length of the EA against the LW, due to the elastic mechanical properties of the EA. In addition, the bending can be reversed so that the EA can also be steered through the CH in RW-style insertions. Steering EAs that are initially inserted through the RW poses a unique challenge in that the EA tip must first be bent away from the medial wall (MW) of the CH before later being bent away from the LW of the cochlea's first turn (Fig. 1). To our knowledge, this has never been attempted previously. The primary reason is that steerable EAs, both experimental prototypes and perimodiolar versions used in the clinic, have been designed with a preferred direction of curvature matching that of the cochlea's first turn and is better suited for the straight, initial trajectory accomplished through a CO. With RW insertions, however, the initial entry angle places the EA tip near the MW, very close to the BM and the OSL. Properly steering the EA through this section would require a curvature direction opposite the remainder of the insertion, which is not possible with existing steerable EAs. In contrast, our method can apply torque in either direction, bending the tip away from either wall as needed, and requires minimal modification to the tip of existing LW EAs.

A detailed explanation of the physics behind our strategy is described in our previous work (31), and is only summarized here. The actuation method uses an external magnet (EM) to apply bending torque to the tip of an EA. The EA is equipped with a permanent magnet rigidly embedded in, or attached to, its tip such that its magnetic dipole (i.e., the vector that points from the

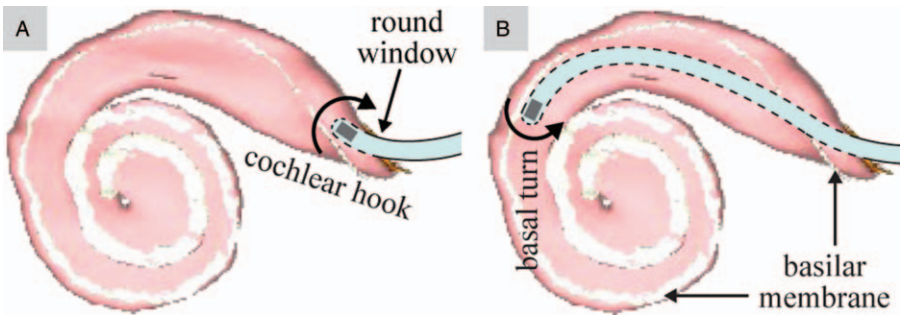

FIG. 1. The ability to steer an EA (modified with a magnet at its tip) through the cochlear hook (*A*) and the basal turn of the cochlea (*B*) requires the EA to bend in opposite directions. The scala-tympani model depicted here, with the basilar membrane shaded in white, is generated from software provided to the public by Eaten-Peabody Laboratory (Boston, MA). EA indicates electrode array.

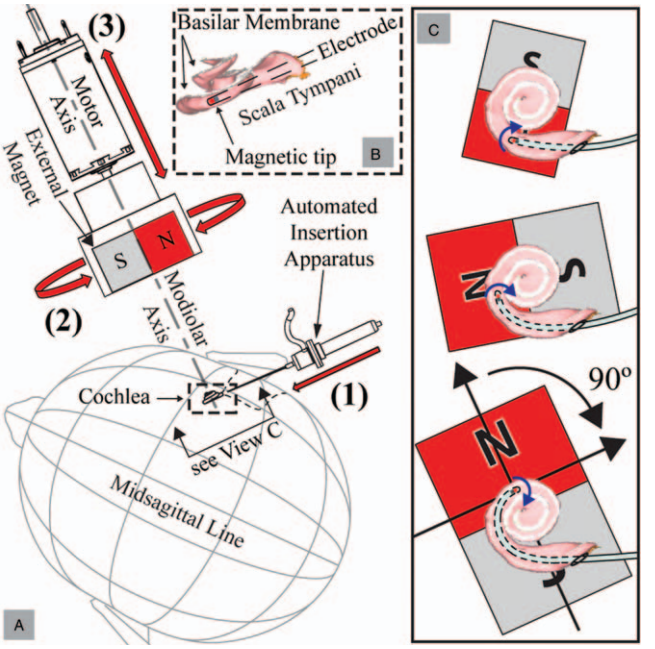

FIG. 2. *A*, Magnetically guided insertions are achieved using three controlled degrees-of-freedom: 1) insertion of an EA with a magnetic tip, 2) rotation of the EM about the modiolar axis, and 3) translation of the EM along the modiolar axis. *B*, Close-up view of the scala tympani with the basilar membrane labeled (and shaded in white) so as to show its location relative to the EM and the EA magnet. *C*, At each step of the insertion, the EM applies torque (shown as blue curved *arrows*) to the EA's magnetic tip, bending the tip away from the LW. To minimize any attractive force on the tip toward the EM, the angle between the magnetic orientations (represented by black *arrows* in the lower-right image pointing from each magnet's south pole to north pole) is maintained at approximately 90 degrees. The increasing size of the EM indicates that it is advancing toward the cochlea and generating increasing torque on the EA's tip. Scala-tympani images are generated from software provided to the public by Eaten-Peabody Laboratory (Boston, MA). EA indicates electrode array; EM, external magnet.

magnet's south pole to its north pole) is aligned with the long axis of the EA. In the arrangement shown in Figure 2, the applied torque is dynamically changed during operation as follows. As the EA is continuously inserted into the cochlea using an automated insertion device, the EM is rotated so that its magnetic field is orthogonal to the lumen at the location of the EA tip, resulting in the magnetic field applied to the EA tip leading the tip magnet by 90 degrees, which is the configuration for maximum magnetic-torque generation on the tip. Simultaneously, the distance between the EM and the EA tip is adjusted to modify the strength of the magnetic field and cause the EA tip to bend away from the LW. As an added benefit, magnetic forces are approximately zero in this configuration and can be neglected. In practice, the rotation of the EM can be preplanned by segmenting the cochlea (32) to determine the lumen heading as a function of insertion depth. This will generate an optimal trajectory for the EM and the automated insertion device. Both the devices can then be aligned with respect to the cochlea by registering them with respect to bone anchors on the patient.

The amount of bending torque needed is based on the EA stiffness and is expected to be unique to the specific model. Since EA flexibility is a design parameter (1), in practice, the necessary bending torque can also be determined as a function of insertion depth. The translation of the EM relative to the cochlea (as illustrated in Fig. 2) can be preplanned based on the required torque throughout the insertion. If the motion of the EM is parameterized by the insertion depth at the proximal end, the entire procedure can be completely preplanned for automated insertions that do not require real-time localization of the EA tip relative to the cochlear walls.

Our previous work (31) suggests that magnetic guidance can reduce insertion forces; however, experiments were conducted with 3-to-1 scale dummy EAs. Progress toward clinical translation requires that similar yields be achievable with at-scale clinical EAs in higher fidelity phantoms (33). This article presents the first attempt at steering actual clinical EAs, modified to have a magnetic tip, using magnetic guidance. We find that magnetic guidance results in a statistically significant reduction in insertion forces for all of the EAs tested, in both cochleostomy and round-window insertions. Further, bidirectional steering through a simulated RW opening is demonstrated for the first time. Finally, accurate estimates of the magnetic field strength necessary to accomplish guided insertions are a direct result from the experiments described herein; this information is necessary to inform the design of a clinical magnetic-guidance system.

Insertion-force reduction is the primary metric for this study, which has been used by numerous groups to initially evaluate prototypes and insertion techniques (3,5,6,8,34,35), particularly in the early stages of

development where the complexity and expense of using cadaveric cochleae is not yet warranted. Although insertions in temporal-bones are preferable in that histology can provide visualization of the final position of the EA and grades of intracochlear damage (36) that might have occurred during the insertion, the complexity of histology and limited access to temporal bones make insertion-force measurements in a transparent ST phantom a reasonable first step.

METHODS

An automated benchtop experimental apparatus was constructed (Fig. 3). EAs, mounted to a robotic linear stage (Fig. 3-1), are inserted into a ST phantom through a simulated RW opening or CO (not shown in Fig. 3) (33). Grid markers are engraved into the phantom and spaced at 30 degrees increments from the RW as suggested by Verbist et al. (37). Insertion forces are measured by mounting the phantom rigidly to a magnetically insensitive force-torque sensor (Fig. 3-3). The motion of the EM (Fig. 3-4) is coordinated with the insertion of the EA using a computer that is programmed with preplanned trajectories before experiments. Translation of the EM is accomplished with a robotic linear stage (Fig. 3-5) while a geared servo-controlled DC motor (Fig. 3-6) rotates the EM. To isolate the force-torque sensor from the motion of the actuators, the EM is mounted on a completely separate platform (Fig. 3-7), and the EA-insertion assembly is mounted on an optics bench that sits on sorbothane pads (Fig. 3-8). A camera system (Fig. 3-9) captures video of the insertion experiment. The rotation axis of the EM is aligned with the central (modiolar) axis of the ST model (shown by the dashed line in Fig. 3). The entry angle for RW trials (Fig. 3-10) was determined by trial-and-error to produce reliable insertions and is within the range of values (4 degrees to 25 degrees) used for insertion experiments in cadaver heads by Wimmer et al. (38). For CO trials, the angle is 0 degree.

The force-torque sensor used is an ATI (Apex, NC) Nano17 Titanium, factory calibrated to ATI's SI-8–0.05 specification. This yields a force resolution of 1.5 mN for all three axes. A tool transform is implemented in software so that the measurements correspond to the origin of the phantom's coordinate system (Fig. 3-2).

N52-grade NdFeB magnets were obtained from SuperMagnetMan (Birmingham, AL). The EM is a cube of 50 mm side length with an estimated dipole moment of 131 A m^2. As implemented in our apparatus, the maximum magnetic field that can be generated at the center of the ST phantom is 225 mT. Cylindrical axially magnetized magnets (0.25 mm diameter by 0.41 mm length, with an estimated dipole moment of 2.4×10^{-5} A m^2) were selected to fit into the tips of the EA used in this study.

All EAs used (Fig. 4) were provided by MED-EL (Innsbruck, Austria). They consisted of three EAs with magnets (labeled E1, E2, and E3) and two unmodified reference EAs (labeled R1 and R2). In two of the three EAs with magnets (E1 and E2), the silicone rubber used to encapsulate the magnet into the tip required a shore-hardness of 90, approximately twice the shore-hardness of the rest of the EA. This was necessary to prevent the magnet from rotating inside the tip during experiments, as the standard silicone rubber was not strong enough to securely fix the magnet when torque was applied by the magnetic field. Only the Flex24 EA with two magnets (E3) was the same actual EA used in both studies (CO and RW). EAs E1 and E2 used for the RW trials are different than EAs E1 and E2 used in the CO trials.

Guided insertions of the EAs with magnets are accomplished using a supervised automated procedure and involve a three-step sequence that is repeated until the end of the insertion as follows: 1) increment the insertion depth by 0.5 mm, 2) rotate the EM to a depth-specific value stored in a look-up

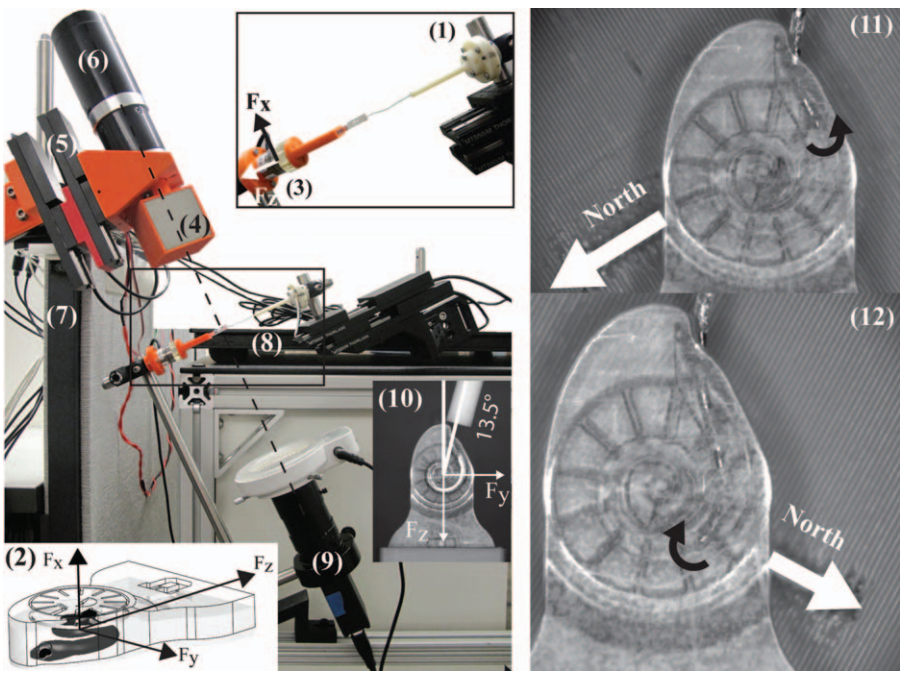

FIG. 3. Experimental setup, with explanations of the various components in the text. To achieve opposite bending torque (black curved *arrows*), the north axis of the EM must be correctly oriented relative to the magnetic tip. EM indicates external magnet.

	Reference	1 magnet	2 magnets	Length
Flex[20]	R1	E1*	---	20 mm
Flex[24]	R2	E2*	E3	24 mm

* with stronger silicone rubber at the tip

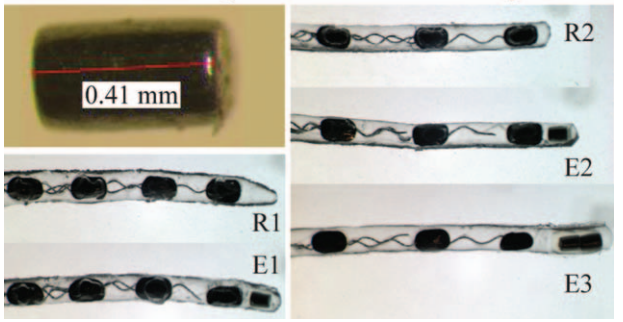

FIG. 4. Modified MED-EL EAs used in this study.

table, and 3) translate the EM relative to the phantom using a depth-specific value stored in a look-up table. Before each insertion, the phantom is filled with saline solution (35) and a small amount of silicone lubricant (34,39) is applied to the electrode tip.

To obtain the values stored in the two look-up tables, before conducting the experiments, the motion of the EM was coordinated to the EA insertion as follows. Each EA was inserted into the phantom at 0.5 mm increments. After each increment, a camera was used to visualize the lumen direction at the current location of the EA tip, and the EM was rotated such that its dipole was orthogonal to the lumen direction, which would cause its applied field to lead the dipole of the EA's tip magnet by 90 degrees. Then, the distance between the EM and the phantom was adjusted until the EA tip was centered in the channel. This procedure was repeated for each EA tested to create EA-specific look-up tables. In addition, to simulate supervisory control of the surgeon throughout the three-step insertion sequence (i.e., the system awaiting surgeon consent between steps in the sequence), the actuators were kept still for one full second between each step. For the RW trials only, the torque is applied in the opposite direction of that found through the CH (Fig. 3-11 and 3-12) after the path curvature reverses. For the control group, we insert the EAs with magnets in 0.5 mm increments and with the EM stationary and positioned far away from the EA. In addition to measured insertion forces, we observe the behavior of the EA to assess if this strategy achieves steering through the CH and the basal turn within the same insertion. There was no attempt to randomize the insertion order between guided and nonguided trials.

RESULTS

All angular insertion depth measurements locate the EA tip with respect to the RW. All linear depth measurements represent movement of the insertion stage. At 0 mm linear insertion depth, the insertion stage positions the most apical electrode band just outside the ST channel. Entering through the RW rather than a CO adds about 1 mm to the path. For clarity, we define ''first turn'' as the section of the lumen from 120 degrees to 210 degrees, measured from the center of the RW.

Magnetic-field and insertion-force values measured for the CO and RW trials are compiled in Figures 5 and 6, respectively, and are the averaged sensor values for every 0.5 mm of EA insertion (to reduce sensor noise). In both the figures, the top row shows the applied magnetic field $\|\mathbf{B}\| = \sqrt[2]{B_x^2 + B_y^2 + B_z^2}$ used to achieve the guided insertions, and measured insertion forces $\|\mathbf{F}\| = \sqrt[2]{F_x^2 + F_y^2 + F_z^2}$ (with 95% confidence levels shown as shaded regions) and *t*-test analysis of the insertion-force difference $\Delta\|\mathbf{F}\|$ are placed below the respective magnetic-field profiles with markers indicating where along the insertion the null hypothesis can be rejected with 95% confidence (i.e., where we are 95% confident that the difference observed is not random). $\Delta\|\mathbf{F}\|$ is computed by subtracting magnetically guided measurements of $\|\mathbf{F}\|$ from nonguided measurements of $\|\mathbf{F}\|$. The number of trials conducted for each EA tested is indicated in the legend. To our knowledge, applying *t*-test analysis to compare insertion-force measurements has never been used in any publication that reports insertion-force measurements, and in our opinion, is an improvement over the conventional reporting of mean and standard deviation.

The results from the *t* tests indicate that magnetic guidance did significantly reduce insertion forces for all EAs tested, though with varying results. In the CO trials (Fig. 5A), the greatest improvements were achieved with E2, with negligible forces up to approximately 17 mm insertion depth and percent reduction at certain locations thereafter greater than 50%, followed by the results for E3. However, we note that the maximum required magnetic field applied to E2 was more than double that applied to E3, due to the larger magnetic dipole embedded in the tip of E3. Only modest reductions in insertion forces were achieved with E1. We determined that the magnitude of the magnetic field required for CO insertions was in the range of 77 to 225 mT, depending on the type of EA and the embedded magnets.

To visualize a typical guided insertion through a CO, image snapshots of E2 are shown in Figure 5B. With this method, the tip is able to reach approximately 180 degrees before the apical section of the EA contacts the LW. Beyond this location, the applied torque is only able to pull the tip away from the LW while the remainder of the EA slides along the LW. However, recall that, due to the mechanical properties of the EA, we know that the pressure is reduced along the entire length of the EA due to the torque at the tip; the net effect is observed in the reduced insertion force. The manner in which the guided E2 contacts the LW is shown through a sequence of images demonstrating the initial contact provided in Supplemental Digital Content 1, http://links.lww.com/MAO/A594. Two things should be noted. First, the EA tip never directly contacts the LW through

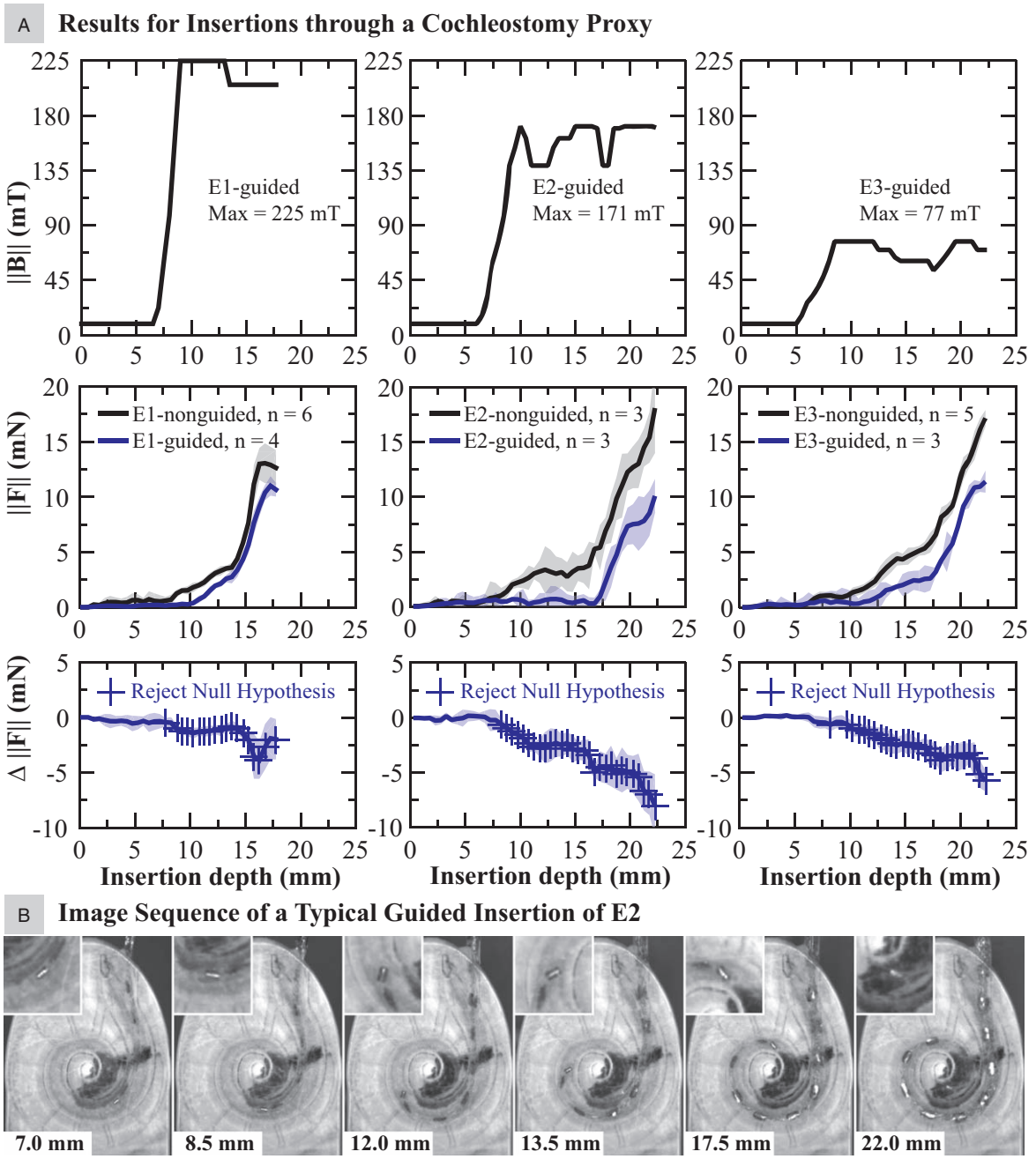

FIG. 5. *A*, Results for applied magnetic field and insertion forces, comparing nonguided and magnetically guided insertions of the EAs with embedded magnets via the cochleostomy proxy. *B*, Images chosen to represent a typical guided insertion of an EA with magnet (E2 in this example) wherein the tip is navigated through the first turn.

the first turn (120–210 degrees). Second, the initial contact between the EA and the LW is no longer concentrated at the tip, but is distributed over the apical section of the EA.

In the RW trials (Fig. 6A), insertion-force reduction was consistently achieved by E3 beyond 10 mm with near 50% reduction at several locations including the end. E2 also consistently achieved statistically significant insertion-force reduction, though not until about 14 mm, with near negligible insertion forces between 14 and 17 mm insertion depth (240–315 degrees). Between 17 and 18 mm, the insertion force reduction, though seemingly large, is not statistically significant because a large stick-slip event occurred during one of the trials of E2-nonguided, causing the insertion force to spike to 26.1 mN. We consider stick-slip as the temporary ''digging'' of the tip into the LW as it slides along the surface, which halts the tip progression and yields a temporary increase in insertion forces until the tip breaks free and resumes sliding. This has the effect of expanding the confidence

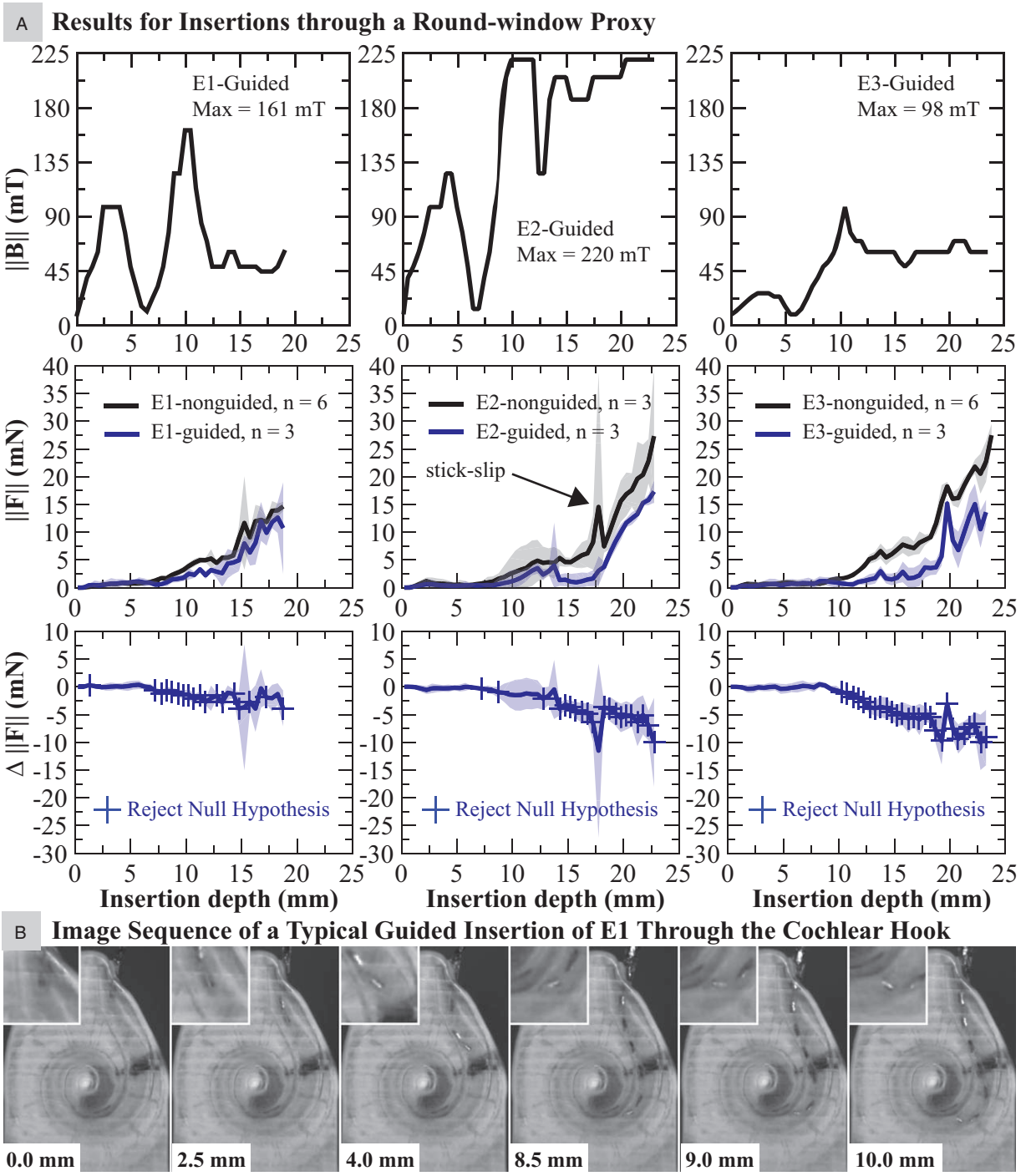

FIG. 6. *A*, Results for applied magnetic field and insertion forces, comparing nonguided and magnetically guided insertions of the EAs with embedded magnets via the round-window proxy. *B*, Images chosen to represent a typical guided insertion of an EA with magnet (E1 in this example) wherein the tip is navigated through the cochlear hook and the first turn.

intervals and increasing the threshold for rejecting the null hypothesis. However, this is the very type of occasional traumatic event that we would like to mitigate through magnetic guidance. If we consider the force increases due to stick-slip at 19 mm for E3-guided, the force increase was consistent for all trials, yielding smaller confidence intervals and a lower threshold to reject the null hypothesis. The maximum magnetic field applied to E2 was more than double that applied to E3, due to the larger magnetic dipole embedded in the tip of E3. Insertion-force reduction was achieved with E1 beyond 7 mm, though less pronounced. Finally, there

is no significant difference in insertion force at the CH between nonguided and guided insertions through the RW, even though direct tip contact is avoided in the guided insertions. We determined that the magnitude of the magnetic field required for RW insertions was in the range of 98 to 220 mT, depending on the type of electrode and the embedded magnets, which is approximately the same as the values required for CO insertion; this suggests that a single-clinical magnetic-guidance system could be designed to enable both CO and RW insertions.

In a RW insertion, a sequence of images visualizing a typical guided insertion of E1 through the CH and entering the first turn is provided in Figure 6B. In all EAs with magnets tested, the tip is guided successfully through the CH, eliminating direct tip contact with the MW (Fig. 6B, images 1–3). As the EA enters the first turn, the torque is reversed successfully so that direct tip contact with the LW is also eliminated (Fig. 6B, images 4–6). But unlike the CO trials wherein each guided EA managed to avoid contact with the LW until the tip reached about 180 degrees, in the RW trials this location is EA dependent. It was determined to be about 135 degrees, 150 degrees, and 180 degrees for E1, E2, and E3, respectively. This implies that entering directly into the lumen via the CO provides more consistent avoidance of the LW. This can be verified by comparing Figure 6B (6) for E1 with Supplemental Digital Content 2, http://links.lww.com/MAO/A595 (B-3 and D-3) for E2 and E3.

We have compiled a video (see Supplemental Digital Content 3, http://links.lww.com/MAO/A596, and 4, http://links.lww.com/MAO/A597) demonstrating both nonguided and magnetically guided insertions in CO and RW openings.

DISCUSSION

Evaluation of our hypotheses is based on *t*-test analysis of the difference between measured insertion forces. Although this does not enable us to make conclusions about future EAs with magnets (since that would require a population study), the process to produce these EAs with magnets can be made repeatable; which gives us reason to think that similar results will be achievable in the future.

Magnetically guiding the EAs reduced insertion forces for all EAs tested, although the improvement for E1 was minimal. It seems that the 20 mm EA, as currently designed, may not be a good candidate for our magnetic-guidance concept. Results achieved through magnetically guiding E2 through a CO are comparable to the best results achieved with perimodiolar EAs inserted with the advance-off-stylet technique (6,8). The results with E3 showed good overall force reduction and also come with the benefit of requiring a smaller EM.

Mechanisms designed to achieve steerable EAs typically increase their stiffness (40). In particular, standard insertions of stylet-based EAs (i.e., not advanced off the stylet) seem to produce maximum insertion forces that are five times greater (6,8) than LW EAs (34,41). Our approach requires only a minor modification to the EA tip and will not compromise the flexibility of LW EAs. To test this, insertion experiments were conducted comparing the reference EAs (i.e., without embedded magnets) against their magnetically tipped counterparts, with all EAs inserted at a constant speed of 0.2 mm/s and without the use of magnetic guidance. The results, provided as Supplemental Digital Contents 5, http://links.lww.com/MAO/A598, and 6, http://links.lww.com/MAO/A599, show minimal insertion-force difference between the EAs compared. The only exception is if the modification alters the tip shape. In these cases (R1 versus E1 in both CO and RW trials), the stick-slip behavior of the EA tip is also altered, though unpredictably.

A benefit of using LW EAs is that they do not have a preferential curvature direction. This eliminates the need to properly align the EA's preferential curvature before insertion as is required with perimodiolar models. Further, a known problem for perimodiolar EAs is that any torsion that twists the EA causes it to be no longer aligned properly to curl away from the LW (11); this is not an issue here because the magnetic dipole at the EA tip is symmetric about the long axis of the EA. Magnetic guidance will not be affected by EA twisting before or during the insertion. However, magnetic guidance will require the EM to be properly aligned with respect to the cochlea, which will require the use of image guidance.

The limitations of insertion-force metrics are worth discussing. In our opinion, this type of metric is most appropriate when used for comparing the relative flexibility among competing EAs or the relative differences in insertion techniques. Absolute sensor values cannot be used to determine potential trauma on intracochlear structures such as the BM, even if the force threshold of the membrane is known (42), because it is unlikely that the force sensor will correctly estimate the tip-contact force. As an example, the EA tip visibly contacts the MW of the CH in all nonguided insertions through the RW (Supplemental Digital Content 6, http://links.lww.com/MAO/A599), yet without any detectable jump in the force-sensor reading. Examples of this behavior are presented in the videos submitted as Supplemental Digital Content 3, http://links.lww.com/MAO/A596, and 4, http://links.lww.com/MAO/A597. This is consistent with findings from a study in which BM perforation was undetected in a temporal-bone specimen mounted directly to an identical force sensor to that used in our studies (35).

Although there was no difference in insertion forces between guided and nonguided EAs in the CH region, by eliminating direct tip contact with the MW immediately after entry through the RW, we hypothesize that one potential trauma site to the BM and the OSL (43) can be eliminated through our technique. In a typical nonguided insertion, the EA tip is directed toward these delicate structures upon entry through the RW. As demonstrated in the guided insertions, the tip is directed down the lumen immediately and made to avoid the MW in the CH.

In addition, optimized insertion vectors, along with the necessary drilling often required to achieve them (15,22), would likely be less crucial.

A second site of potential trauma (43,44) is along the first turn, where contact with the LW sometimes deflects the EA tip out-of-plane into the BM. To avoid this type of impingement, the EAs are navigated successfully so that the initial contact is distributed over the apical section of the EA, rather than localized at the tip, and with the tip always directed away from the wall. We hypothesize that this will be less traumatic, and we plan to examine this in future work with temporal bones. The likelihood of incomplete insertions increases dramatically if tip contact with the spiral ligament is severe enough (45). By eliminating direct tip contact with the LW throughout the entirety of the insertion, both of these incidences may be reduced.

In addition, the use of a magnetic field intended to pull the tip of the EA away from the MW and LW has the benefit of providing a passive magnetic spring that attempts to keep the orientation of the tip parallel to the BM, which will further mitigate the risk of the magnetic tip deviating out-of-plane into the BM. That is, by setting the magnetic field at the tip to be on a plane parallel to the BM, any tip deviation from this plane will incur a magnetic torque that pulls (rotates) the tip back onto the plane (Supplemental Digital Content 7, http://links.lww.com/MAO/A600). This protection of the BM, which can be deduced from first principles, cannot be observed in the insertion-force data. The benefit of the passive-magnetic-spring effect should be quantified in future work, possibly by inserting the EA with a nonideal insertion vector.

It should be noted that this passive-magnetic-spring effect, as well as our intended magnetic guidance, both assume that the EM is properly registered (aligned) with respect to the cochlea. If the EM is substantially misaligned, the magnetic field will no longer affect the tip as intended, and there will be some degree of misalignment at which we would expect the ''magnetic guidance'' to do more harm than good. Because the physics of magnetic torque rely on the vector cross product between the EA's tip magnetic dipole and the applied field (i.e., the sine of the angle between them), we expect unintended out-of-plane magnetic torque to follow the small-angle approximation and be negligible for misalignment up to 10 degrees. The sensitivity of our magnetic-guidance method to EM misalignment should be quantified in future work.

In this study, all insertions were conducted after the automated insertion tool was carefully aligned to the phantom opening. However, in a real clinical case, the surgeon can align the tool to the patient with the aid of a commercial optical tracker. For example, Bruns and Webster (46) have demonstrated that an automated insertion tool can be aligned to within 1.06 degrees of the desired insertion trajectory using an image-guided method that can potentially register the tool with respect to the cochlea using bone anchors on the patient.

In our experiments, we generated the insertion profiles offline, and then ran those insertions in an open-loop fashion. For the sake of performing controlled and repeatable experiments, we chose to generate the profiles following a specific procedure, but we do not claim that our procedure results in optimal insertions. In our intended concept, the insertions will be modified in real time using a sensor measuring the force at the location where the insertion stage holds the EA, as has been demonstrated previously (47). This will likely enable improved insertions, as well as monitoring to prevent any unsafe rises in the insertion force.

One of the challenges with insertion-force studies is maintaining the mechanical integrity of the EA while conducting sufficient insertion trials to obtain statistically meaningful results. Since a protocol does not exist, to our knowledge, to guide experimenters with this dilemma, we typically reuse the EA if no damage is visibly detected. In the case of the EAs with magnets, the guided insertion trials were limited to 3 to balance the need for statistics (primarily to conduct *t*-test analyses) with maintaining the mechanical integrity of the magnet at the tip. Typically, we found that the 95% confidence intervals in the guided insertions were only 2 to 3 mN. This is indicative of very repeatable insertions, and in our opinion, additional trials likely would not have affected the averaged insertion forces appreciably. In addition, even the relatively few runs were already sufficient to prove a significant benefit of magnetic guidance.

Finally, E3 was (unintentionally) made with a substantial gap between the embedded magnet and the distal electrode band (see Fig. 4), and we observed substantial bending in the gap region, which has low stiffness due to the lack of any wires to act as an elastic backbone. This is undesirable as it resulted in an artificial limit to the applied torque we were able to apply to pull the EA away from the LW before risking a collision of the tip with the MW (Supplemental Digital Content 2, http://links.lww.com/MAO/A595, Image Series C). In future prototypes, it should be a priority to embed the tip magnet close to the distal electrode band.

CONCLUSION

In this study, we demonstrated that magnetic guidance of a robotically inserted lateral-wall cochlear-implant electrode array equipped with a permanent magnet at its tip results in a statistically significant reduction in insertion forces compared with robotic insertion without magnetic guidance, for both cochleostomy and round-window insertions. To our knowledge, this is the first attempt at actively steering clinical-type electrode arrays of any type through both the cochlear hook and the first turn. Direct tip contact at the medial wall of the cochlear hook and at the lateral wall of the first turn was eliminated while maintaining the inherent safety of flexible lateral-wall electrode arrays. Insertion-force reduction was greatest with the 24 mm electrode array, and less pronounced with the 20 mm electrode array. We found

that it is feasible to embed permanent magnets in the tip of clinical electrode arrays, but that care should be taken to embed them close to the distal electrode band. We determined that clinical magnetic-guidance systems should be designed to generate magnetic fields at the cochlea with strengths of least 98 mT, and if possible as high as 225 mT.

Acknowledgments: The authors gratefully acknowledge support from Anandhan Dhanasingh of MED-EL for fabricating the electrodes used in these experiments.

REFERENCES

1. Jolly C, Garnham C, Mirzadeh H, et al. Electrode features for hearing preservation and drug delivery strategies. *Adv Otorhinolaryngol* 2010;67:28–42.
2. Nguyen Y, Mosnier I, Borel S, et al. Evolution of electrode array diameter for hearing preservation in cochlear implantation. *Acta Otolaryngol* 2013;133:116–22.
3. Min KS, Oh SH, Park M, Jeong J, Kim SJ. A polymer-based multichannel cochlear electrode array. *Otol Neurotol* 2014;35: 1179–86.
4. Radeloff A, Unkelbach MH, Mack MG, et al. A coated electrode carrier for cochlear implantation reduces insertion forces. *Laryngoscope* 2009;119:959–63.
5. Majdani O, Schurzig D, Hussong A, et al. Force measurement of insertion of cochlear implant electrode arrays in vitro: Comparison of surgeon to automated insertion tool. *Acta Otolaryngol* 2010;130: 31–6.
6. Roland JT Jr. A model for cochlear implant electrode insertion and force evaluation: Results with a new electrode design and insertion technique. *Laryngoscope* 2005;115:1325–39.
7. Schurzig D, Webster III RJ, Dietrich MS, Labadie RF. Force of cochlear implant electrode insertion performed by a robotic insertion tool: Comparison of traditional versus advance off–stylet techniques. *Otol Neurotol* 2010;31:1207–10.
8. Todd CA, Naghdy F, Svehla MJ. Force application during cochlear implant insertion: An analysis for improvement of surgeon technique. *IEEE Trans Biomed Eng* 2007;54:1247–55.
9. Boyer E, Karkas A, Attye A, Lefournier V, Escude B, Schmerber S. Scalar localization by cone-beam computed tomography of cochlear implant carriers: A comparative study between straight and periomodiolar precurved electrode arrays. *Otol Neurotol* 2015;36:422–9.
10. Rebscher SJ, Hetherington A, Bonham B, Wardrop P, Whinney D, Leake PA. Considerations for design of future cochlear implant electrode arrays: Electrode array stiffness, size, and depth of insertion. *JRRD* 2008;45:731–47.
11. Coordes A, Ernst A, Brademann G, Todt I. Round window membrane insertion with perimodiolar cochlear implant electrodes. *Otol Neurotol* 2013;34:1027–32.
12. Briggs RJS, Tykocinski M, Xu J, et al. Comparison of round window and cochleostomy approaches with a prototype hearing preservation electrode. *Audiol Neurotol* 2006;11 (suppl 1):42–8.
13. Gudis DA, Montes M, Bigelow DC, Ruckenstein MJ. The round window: Is it the ''cochleostomy'' of choice? Experience in 130 consecutive cochlear implants. *Otol Neurotol* 2012;33:1497–501.
14. Havenith S, Lammers MJW, Tange RA, et al. Hearing preservation surgery: Cochleostomy or round window approach? A systematic review. *Otol Neurotol* 2013;34:667–74.
15. Roland PS, Wright CG, Isaacson B. Cochlear implant electrode insertion: The round window revisited. *Laryngoscope* 2007;117: 1397–402.
16. Causon A, Verschuur C, Newman TA. A retrospective analysis of the contribution of reported factors in cochlear implantation on hearing preservation outcomes. *Otol Neurotol* 2015;36:1137–45.
17. O'Connor EF, Fitzgerald A. Hearing preservation surgery: Current opinions. *Adv Otorhinolaryngol* 2010;67:108–15.
18. Hassepass F, Bulla S, Maier W, et al. The new mid-scala electrode array: A radiologic and histologic study in human temporal bones. *Otol Neurotol* 2014;35:1415–20.
19. Breinbauer HA, Praetorius M. Variability of an ideal insertion vector for cochlear implantation. *Otol Neurotol* 2015;36:610–7.
20. Briggs RJS, Tykocinski M, Stidham K, Roberson JB. Cochleostomy site: implications for electrode placement and hearing preservation. *Acta Otolaryngol* 2005;125:870–6.
21. Meshik X, Holden TA, Chole RA, Hullar TE. Optimal cochlear implant insertion vectors. *Otol Neurotol* 2010;31:58.
22. Shapira Y, Eshraghi AA, Balkany TJ. The perceived angle of the round window affects electrode insertion trauma in round window insertion: An anatomical study. *Acta Otolaryngol* 2011; 131:284–9.
23. Addams-Williams J, Munaweera L, Coleman B, Shepherd R, Backhouse S. Cochlear implant electrode insertion: In defence of cochleostomy and factors against the round window membrane approach. *Cochlear Implants Int* 2011;12 (suppl 2):36–9.
24. Richard C, Fayad JN, Doherty J, Linthicum FH Jr. Round window versus cochleostomy technique in cochlear implantation: Histological findings. *Otol Neurotol* 2012;33:1181.
25. Adunka OF, Buchman CA. Scala tympani cochleostomy I: Results of a survey. *Laryngoscope* 2007;117:2187–94.
26. Fraysse B, Maclias ÁR, Sterkers O, et al. Residual hearing conservation and electroacoustic stimulation with the nucleus 24 contour advance cochlear implant. *Otol Neurotol* 2006;27:624–33.
27. Todt I, Rademacher G, Wagner J, et al. Evaluation of cochlear implant electrode position after a modified round window insertion by means of a 64-multislice CT. *Acta Otolaryngol* 2009;129: 966–70.
28. Wanna GB, Noble JH, Carlson ML, et al. Impact of electrode design and surgical approach on scalar location and cochlear implant outcomes. *Laryngoscope* 2014;124:S1–-7.
29. Jeyakumar A, Peña SF, Brickman TM. Round window insertion of precurved electrodes is traumatic. *Otol Neurotol* 2014;35:52–7.
30. Souter MA, Briggs RJ, Wright CG, Roland PS. Round window insertion of precurved perimodiolar electrode arrays: How successful is it? *Otol Neurotol* 2011;32:58–63.
31. Clark JR, Leon L, Warren FM, Abbott JJ. Magnetic guidance of cochlear implants: Proof-of-concept and initial feasibility study. *J Med Devices* 2012;6:035002.
32. Noble JH, Labadie RF, Majdani O, Dawant BM. Automatic segmentation of intracochlear anatomy in conventional CT. *IEEE Trans Biomed Eng* 2011;58:2625–32.
33. Leon L, Cavilla MS, Doran MB, Warren FM, Abbott JJ. Scala-tympani phantom with cochleostomy and round-window openings for cochlear-implant insertion experiments. *J Med Devices* 2014;8: 041010.
34. Adunka O, Kiefer J, Unkelbach MH, Lehnert T, Gstoettner W. Development and evaluation of an improved cochlear implant electrode design for electric acoustic stimulation. *Laryngoscope* 2004;114:1237–41.
35. Nguyen Y, Miroir M, Kazmitcheff G, et al. Cochlear implant insertion forces in microdissected human cochlea to evaluate a prototype array. *Audiol Neurotol* 2012;17:290–8.
36. Eshraghi AA, Yang NW, Balkany TJ. Comparative study of cochlear damage with three perimodiolar electrode designs. *Laryngoscope* 2003;113:415–9.
37. Verbist BM, Skinner MW, Cohen LT, et al. Consensus panel on a cochlear coordinate system applicable in histologic, physiologic, and radiologic studies of the human cochlea. *Otol Neurotol* 2010;31:722–30.
38. Wimmer W, Bell B, Huth ME, et al. Cone beam and microcomputed tomography validation of manual array insertion for minimally invasive cochlear implantation. *Audiol Neurotol* 2014;19:22–30.
39. Kontorinis G, Paasche G, Lenarz T, Stöver T. The effect of different lubricants on cochlear implant electrode insertion forces. *Otol Neurotol* 2011;32:1050–6.

40. Zhang J, Wei W, Ding J, Roland JT Jr, Manolidis S, Simaan N. Inroads toward robot-assisted cochlear implant surgery using steerable electrode arrays. *Otol Neurotol* 2010;31:1199–206.
41. Helbig S, Settevendemie C, Mack M, Baumann U, Helbig M, Stöver T. Evaluation of an electrode prototype for atraumatic cochlear implantation in hearing preservation candidates: Preliminary results from a temporal bone study. *Otol Neurotol* 2011;32:419–23.
42. Schuster D, Kratchman LB, Labadie RF. Characterization of intracochlear rupture forces in fresh human cadaveric cochleae. *Otol Neurotol* 2015;36:657–61.
43. Carlson ML, Driscoll CLW, Gifford RH, McMenomey SO. Cochlear implantation: Current and future device options. *Otolaryngol Clin North Am* 2012;45:221–48.
44. Zeng FG, Rebscher S, Harrison W, Sun X, Feng H. Cochlear implants: System design, integration, and evaluation. *IEEE Reviews in Biomed Eng* 2008;1:115–42.
45. Lee J, Nadol JB Jr, Eddington DK. Factors associated with incomplete insertion of electrodes in cochlear implant surgery: A histopathologic study. *Audiol Neurotol* 2011;16:69–81.
46. Proc. SPIE 10135, Medical Imaging 2017: Image-Guided Procedures, Robotic Interventions, and Modeling, 101350O (3 March 2017).
47. Schurzig D, Labadie RF, Hussong A, Rau TS, Webster RJ III. Design of a tool integrating force sensing with automated insertion in cochlear implantation. *IEEE ASME Trans Mechatron* 2012; 17:381–9.